SCIENTIFIC REPORTS

OPEN

SUBJECT AREAS:
RAMAN SPECTROSCOPY
NANOPHOTONICS AND PLASMONICS
SERS
ATOMIC AND MOLECULAR INTERACTIONS WITH PHOTONS

Received
9 June 2014

Accepted
7 November 2014

Published
27 November 2014

Correspondence and requests for materials should be addressed to M.S. (mtsun@iphy.ac.cn) or P.W. (pjwang@cnu.edu.cn)

Plasmon-driven dimerization via S-S chemical bond in an aqueous environment

Lin Cui[1,2], Peijie Wang[1], Xiaowei Chen[3], Yurui Fang[4], Zhenglong Zhang[5] & Mengtao Sun[2,1]

[1]The Beijing Key Laboratory for Nano-Photonics and Nano-Structure, Center for Condensed Matter Physics, Department of Physics, Capital Normal University, Beijing 100048, People's Republic of China, [2]Beijing National Laboratory for Condensed Matter Physics, Institute of Physics, Chinese Academy of Sciences, P. O. Box 603-146, Beijing, 100190, People's Republic of China, [3]Departamento de Ciencia de los Materiales, Ingeniería Metalúrgica Química Inorgánica, Facultad de Ciencias, Universidad de Cadiz (Campus Río San Pedro), E-11510 Puerto Real (Cadiz), Spain, [4]Division of Bionanophotonics, Department of Applied Physics, Chalmers University of Technology, Gothenburg SE-412 96, Sweden, [5]Leibniz Institute of Photonic Technology, Albert-Einstein-Str. 9, 07745 Jena, Germany.

The surface-enhanced Raman scattering (SERS) spectra of thioanisole are experimentally investigated in an electrochemical environment in this study. Two Raman peaks, which depend strongly not only on electric potential but also on the local surface plasmon resonances (LSPR), have been observed. Theoretical calculations reveal that thioanisole is first dissociated from thiophenol via the S-CH_3 bond; plasmons then drive the dimerisation of thiophenol via the S-S bond, which is strongly potential dependent. One Raman peak corresponds to the S-S vibrational mode of the thiophenol dimer, and the other corresponds to the asymmetric C-C stretching modes of the benzenyl of the thiophenol dimer. The potential-dependent two Raman modes is the potential-dependent dimerisation dynamics of thiophenol via the S-S bond. Our experimental findings provide insight into the structural elucidation of adsorbed molecules and molecular surface reaction dynamics.

Elucidation of the molecular structure of adsorbed molecules and molecular surface reaction dynamics is among the most important fields in surface science. The ultrasensitive Raman spectrum is one of the most powerful methods for surface adsorbate analysis, not only because of its "finger print" analysis technology on the nanoscale but also because of the enormous local surface plasmon resonance (LSPR) enhancements or charge transfer enhancements of the Raman spectra[1–10].

Recently, plasmon chemistry has become one of the most promising research fields[11–21], and directly plasmon-driven surface catalytic reactions have been experimentally performed. Plasmons are able not only to drive molecular synthesis but also to cleave specific chemical bonds as nano scissors via plasmonic hot electrons[11–21]. In the process of plasmon-driven surface catalytic reactions, certain new Raman peaks appear or certain Raman peaks disappear.

In this work, the SERS spectra of thioanisole were experimentally investigated in an liquid electrochemical environment. Our experimental results revealed that two Raman peaks are not only dependent on electric potential but also strongly dependent on LSPR. Theoretical analysis indicated that thioanisole is first dissociated from thiophenol via the S-CH_3 bond at -0.4 V, and at the same time, these two Raman peaks appeared. These peaks represent the S-S bond of the thiophenol dimer and the asymmetric C-C stretching modes of the benzenyl of the thiophenol dimer. Our results demonstrate that the potential-dependent dimerisation dynamics of thiophenol via the S-S bond. Our experimental findings provide insight into the structural elucidation of adsorbed molecules and molecular surface reaction dynamics.

Results

Figure 1a shows the Ag substrate before it was roughened. Figure 1b and 1c show SEM images of roughened Ag substrates at different magnifications. Figure 1c demonstrates that the surface of the roughened Ag substrate consists of 3-dimensional (3D) "hot" spots of nanoparticles, which can produce stronger electromagnetic enhancements and more "hot" spots[22–25], indicating that the roughened Ag substrate is more suitable for the

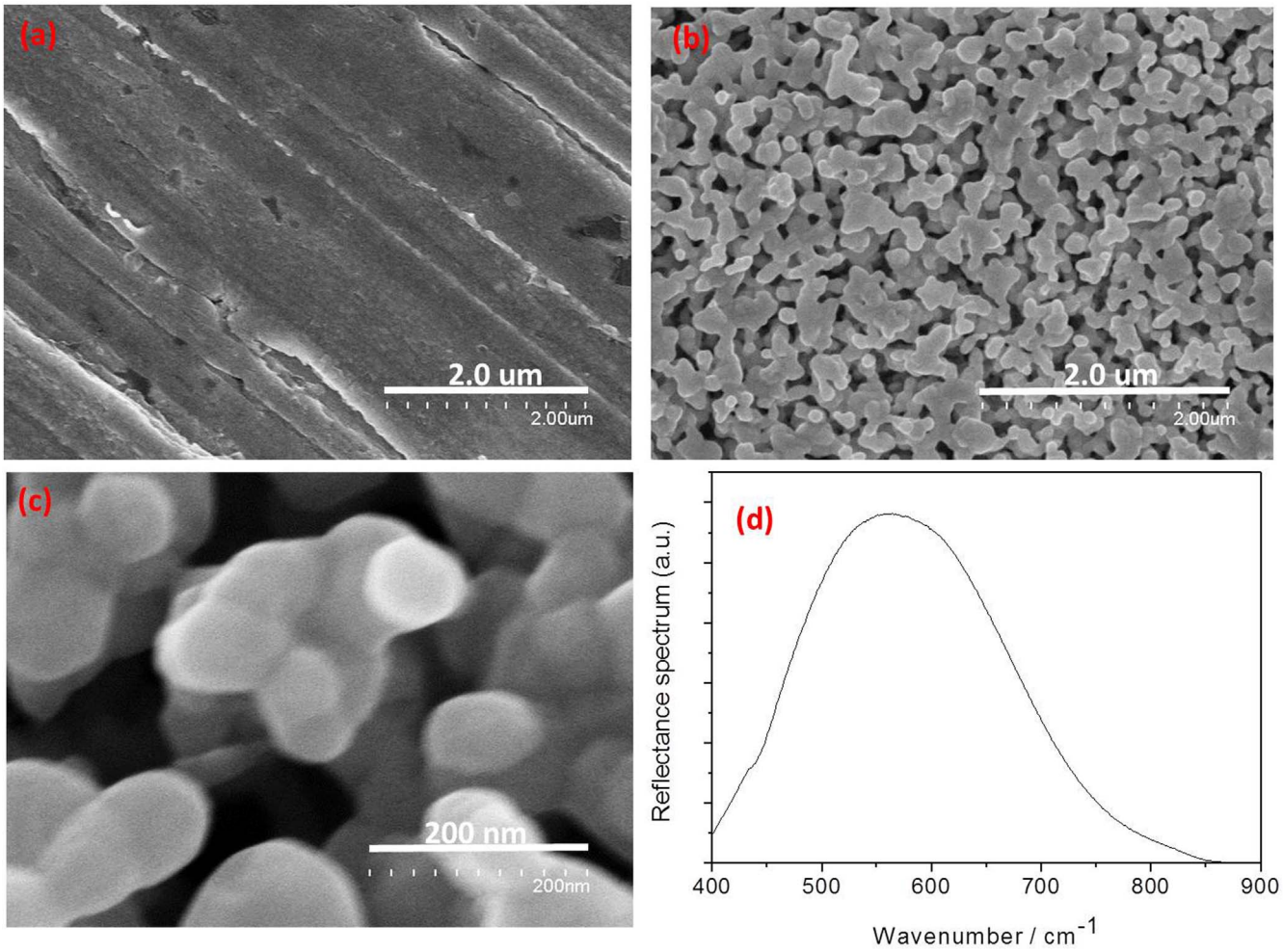

Figure 1 | Characterisation of the Ag substrate. (a) SEM images of the Ag substrate without roughening; (b) and (c) SEM images of roughened Ag substrates at different magnifications; (d) reflectance spectra of roughened Ag substrates.

measurement of SERS. Figure 1d shows the reflectance spectrum of roughened Ag substrates. The LSPR peak is approximately 532 nm, but the LSPR at approximately 785 nm is very weak.

The data presented in Fig. 2(a) displays as an increase in overall intensity of the bands as function of potential, due to the increase of LSPR by increasing the voltages. Here, we focused on the Raman intensities at 464 and 1584 cm^{-1} at different voltages, since they are potential-driven potential-dependent new Raman peaks. At low electric voltage, these two peaks do not appear (there are no such Raman peaks at all at low voltages), whereas with increasing electric voltage, the intensities of these two Raman peaks are gradually selectively enhanced. For a deeper understanding of the above results excited at 532 nm, the electric voltages were also gradually decreased from −1.2 V to 0 V. The data presented in Fig. 2(b) demonstrates as a decrease in overall intensity of the bands as function of potential. When the Raman intensity at 1076 cm^{-1} in different voltages are normalized, the Raman intensities at 1584 cm^{-1} at different voltages are also potential-dependent decreased. However, these Raman peaks did not disappear as expected (see Fig. 2b). This phenomenon revealed that with the decrease of the potential voltages, the LSPR intensity is also decreased. The Raman peaks at 464 cm^{-1} was almost not decreased in Fig. 2(b). The Raman peaks at 464 cm^{-1} was increased only with the increase in potential voltage, but did not decrease when the voltage was decreased again. Theoretical calculations demonstrated that Raman mode at 464 cm^{-1} was the S-S bond; therefore, this is not a reversible process for the dimerization (it will be discussed later in detailed).

The changing tendencies of these two newly formed Raman peaks at 464 and 1584 cm^{-1} via potentials can be seen in Figure 2c and 2d, respectively. It was found that the intensities of these two Raman modes are strongly dependent on the electric potentials, although they follow different rules. For the case of 464 cm^{-1}, from 0 v to −0.4 V, there is no such Raman peak, while from −0.4 v to −0.6 V, this Raman peak increases sharply. In addition, from −0.6 V to −1.2 V, this Raman peak increases gradually. In comparison, the intensity of the Raman peak at 1584 cm^{-1} gradually increases from 0 V to −0.9 V, then increases sharply from 1.0 V to −1.2 V.

The cyclic voltage sweep V-I curve was measured (see Fig. 3) to study the nature of the appearance of these two increased Raman peaks when the potential is greater than −0.4 V. The results indicated a strong peak at approximately −0.4 V; therefore, there are chemical reactions under this experimental condition. The most likely explanation is that thioanisole was first dissociated from thiophenol via the S-CH_3 bond at −0.4 V, while the plasmon-driven formation of the S-S bond of thiophenolled to the formation of a thiophenol dimer, which was potential dependent. With increasing voltage, the probability of dimerisation gradually increased, as shown in Figure 2a, with excitation at 532 nm.

Theoretically, the Raman spectra of thioanisole and the thiophenol dimer were calculated using a quantum chemical method. First, the calculated Raman spectrum of thioanisole was compared to the experimental SERS spectrum at a low voltage (−0.2 V); see Figure 4a. The theoretical calculated Raman spectrum of thioanisole

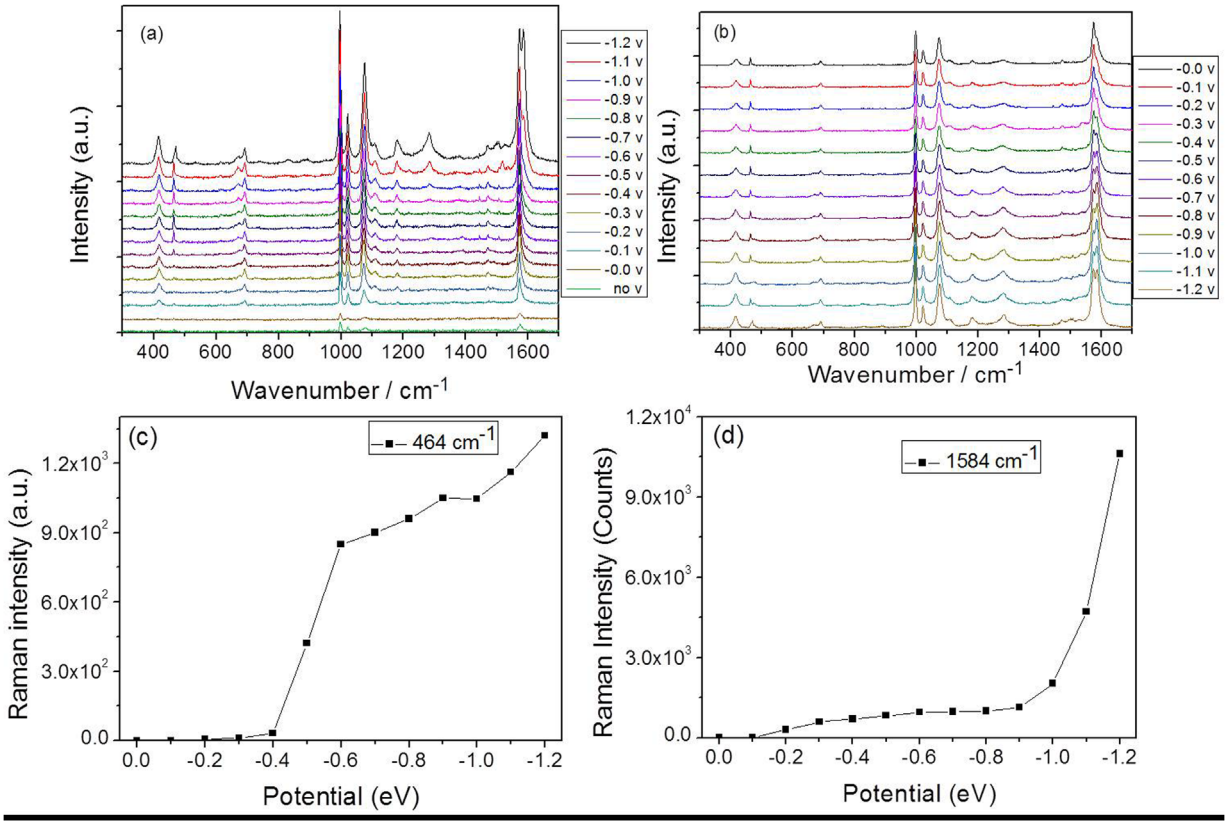

Figure 2 | Potential-dependent SERS spectra excited with a 532-nm laser. (a) The potential-dependent SERS spectra from 0 to −1.2 V and (b) the potential-dependent SERS spectra from −1.2 to 0 V.(c) and (d) Changing tendencies of Raman peaks at 464 and 1584 cm^{-1}according to the potential, where the mean error is within 5%.

is highly consistent with experimental SERS at −0.2 V, and there is no vibrational mode at 464 cm^{-1} at all, and only one Raman peak at 1573 cm^{-1}; furthermore, the vibrational mode at 1573 cm^{-1} can be attributed to the C-C stretching mode of the benzenyl of thioanisole. Next, the comparison of the calculated thiophenol dimer with the experimental SERS at high voltage, −1.2 V, can be seen in Figure 4b. We also found that the Raman peak at 464 cm^{-1} represents the S-S stretching mode of the thiophenol dimer, and the two experimental Raman peaks at 1573 and 1585 cm^{-1} represent the almost degenerated C-C symmetric and asymmetric vibrational modes of the benzenyl of the thiophenol dimer, respectively. These three vibrational modes can be seen in Figure 4c. Due to the interaction between molecule and substrate, and the higher potential voltages (larger plasmon enhancement), these two almost degenerated Raman peaks at 1573 and 1585 cm^{-1} are slightly splitted, and then they can be observed experimentally at higher potential voltages. The data presented in Fig. 2(b) demonstrates that the Raman intensities at 1584 cm^{-1} at different voltages are also potential-dependent decreased, which revealed that the coherence degree of these two almost degenerated Raman modes is decreased with the decrease of potential voltages (weaker LSPR intensity) again. However, these increased Raman peaks did not disappear as expected (see Fig. 2b); moreover, the Raman peak at 464 cm^{-1} (S-S stretching mode) in Fig. 2(b) is not decreased at all, which revealed that the dimerisation is still stable.

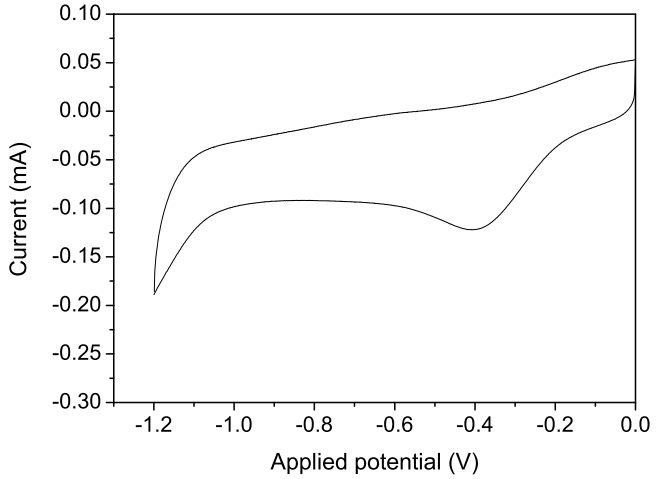

Figure 3 | Potential-dependent cyclic voltammograms of thioanisole.

To study the relationship between LPSR and the dimerisation process, SERS spectra excited at 785 nm were also recorded. Owing to the weak LSPR at approximately 785 nm (see Fig. 1d), the increased Raman peaks at 464 and 1585 cm^{-1} (in Fig. 2a) cannot be observed in Figure 5, as the required laser intensity is 8.5 times larger than the intensity of the 532 nm laser. It can be concluded that the dynamics of dimerisation depend on two parameters:1) the raised Fermi level based on the applied electric voltage and 2) strong LSPR. Only the dissociation of the S-CH_3 of thioanisole was observed, but there was no plasmon-driven thiophenol dimer.

Discussion

Figure 6 illustrates the nature of plasmon-driven potential, with the LSPR depending on the molecular reaction dynamics on the Ag surface. Usually, the hot electrons generated from plasmon decay can drive chemical reactions[11–22]. Hot electrons provide kinetic energy and electrons for the chemical reaction, and the reaction barrier can be easier overcome. In the case of laser excitation at 532 nm, without sufficient external potential (below 0.4 V), the

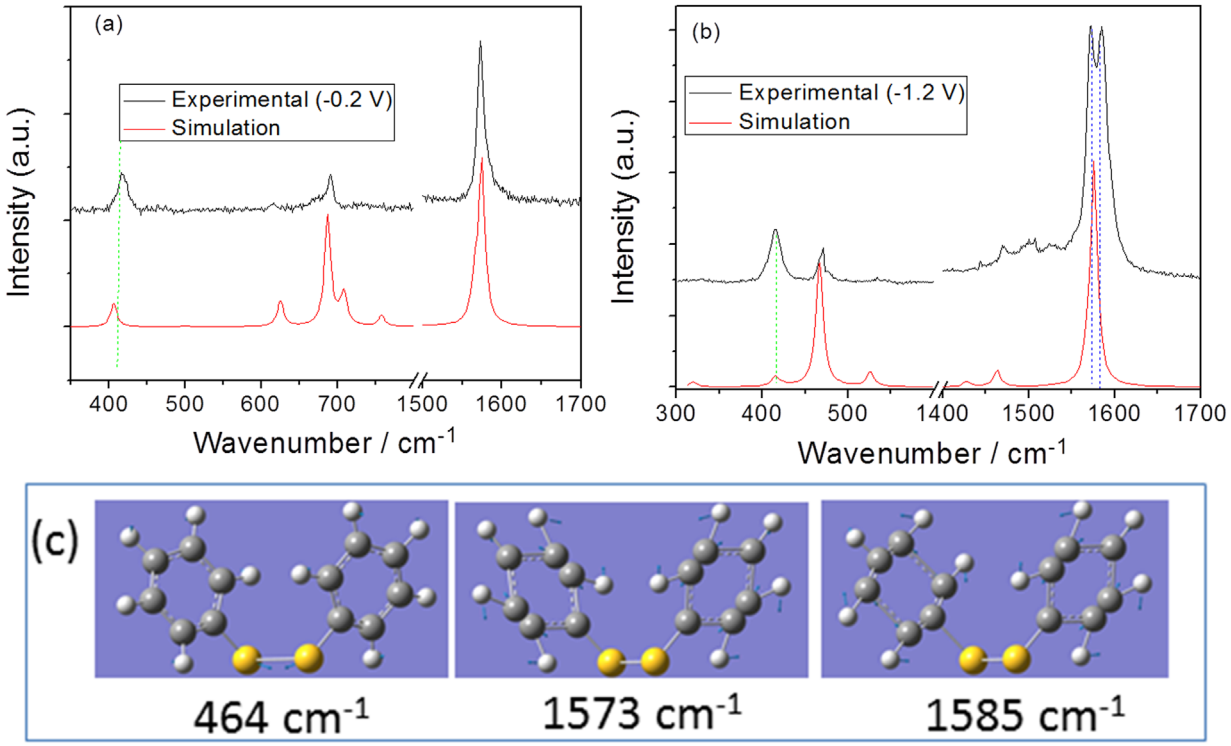

Figure 4 | Experimental and theoretical SERS spectra and molecular vibrational modes. (a) Experimental (from Fig. 2) and theoretical SERS spectra of thioanisole, (b) Experimental and theoretical SERS spectra of the thiophenol dimer. (c) Vibrational modes of the thiophenol dimer.

energies of the laser and hot electrons cannot reach the energy of dimerisation via the S-S bond, even though the LSPR is strong. When the voltage is greater than 0.4 V (raising the Fermi level), the energies of the laser and hot electrons can achieve the energy of dimerisation via the S-S bond of thiophenol, which is enhanced by the strong LSPR. If there is no energy loss, the energy of hot electrons is equal to the laser energy. The electron energy distributions of hot electrons are time dependent following the decay of a plasmon[21,26]. The depicted distributions in Figure 6 are time-averaged distributions[21,26] and resemble a Fermi-Dirac distribution under these continuous wave (CW) illumination conditions[21,26]. Moreover, the magnitude of the Fermi-Dirac distribution is strongly dependent on the intensity of the laser[26]. Due to the non-conservation of momentum in a nanocrystal[26], the carrier distribution has a high energy and occupies the entire region of $E_F < \varepsilon < E_F + \hbar\omega$ in the nanosystem, where E_F is the Fermi energy level. Note that the relationship between the optical absorption energy and the shift of electrode potential can be estimated by[27]

$$E(\Delta V) = E_0(\Delta V = 0) - e\beta\Delta V \quad (1)$$

where $E(\Delta V)$ is the optical absorption energy, ΔV is the change of the cathode potential V and $\beta \leq 1$. In the Helmholtz model, $\beta = 1$[28].

For the case of laser excitation at 785 nm, the total energies (external potential plus hot electrons decayed from LSPR) cannot reach the dimerisation energy; moreover, the LSPR is very weak at 785 nm, and the process of dimerisation cannot o occurs in

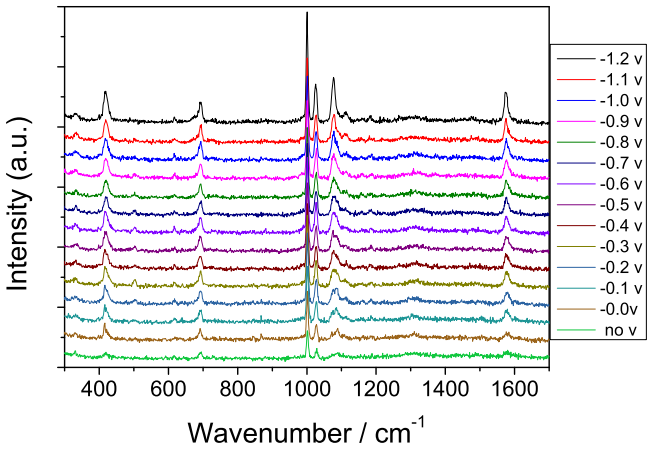

Figure 5 | Potential-dependent SERS spectra excited at 785 nm by a laser with potentials from 0 to −1.2 V.

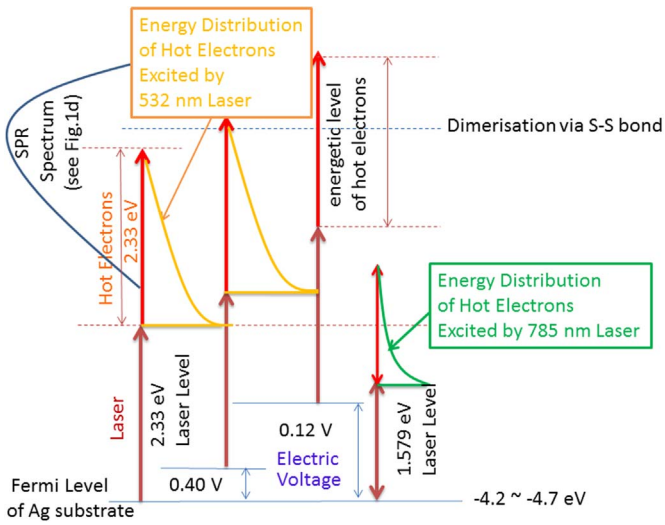

Figure 6 | Scheme of plasmon-driven potential and LSPR-dependent molecular reaction dynamics on the surface. The reflectance spectra of roughened Ag substrates can also be seen in Figure 1d. The Fermi level of the Ag substrate was taken from the CRC Handbook of Chemistry and Physics (2008).

Figure 2c. For this reason, the total energies of the applied potential and hot electrons excited by LSPR are the two most important factors for observing such molecular reaction dynamics on a surface.

In summary, the plasmon-driven potential and LSPR-dependent SERS spectra of thioanisole were investigated experimentally and theoretically. Potential-dependent increased Raman peaks were observed experimentally, and theoretical analysis revealed that these two incresed Raman peaks were potential- and LSPR-dependent Raman peaks, which revealed the dynamics of thiophenol dimerisation, namely the S-S vibration mode at 464 cm^{-1} and the asymmetric C-C stretching mode of the benzenyl of thiophenol at 1587 cm^{-1}. Our experimental results also confirmed that the dimerisation is stably excited by incident 532-nm laser light, as when the voltage was returned to 0 V from −1.2 V, these two Raman peaks could still be observed. A mechanism for these molecular reaction dynamics on the surface was proposed and rationally interpreted.

Note that the orientation of the molecule towards the metallic surface also affects the band ratio, which is known as the surface selection rule. In addition, changes in orientation of the molecule towards the surface are easily altered by changing the potential. However, we can exclude this factor, as these two vibrational modes did not appear in the calculated results (see Fig. 4a), and the two new vibrational modes resulted from the thiophenol dimer (see Fig. 4b). Our work reveals that the intensities of these two Raman modes are strongly dependent on the electric potentials, but with different rules; see Figure2c and 2d. These two newly formed vibrational modes depend strongly on electromagnetic enhancement tuned by electric potentials. In particular, stronger electromagnetic fields are associated with a greater probability of dimerisation, leading to stronger Raman intensities for these two modes.

Methods

Prior to the experiment, the Ag electrode (a single-crystal silver rod of 99.9% purity) was polished with emery paper and cleaned with Milli-Q water in an ultrasonic bath. The electrode was then placed in a typical electrochemical cell containing 0.1 M Na_2SO_4solution for roughening. A double potential step was used to roughen the surface by applying a voltage of +0.25 V for 8 s and then applying a voltage of −0.35 V. This roughening treatment was performed to enhance the Raman intensity for the convenience of spectral recording. After the roughening pre-treatment, the electrode was placed in an electrochemical cell containing 0.1 M KCl and 0.05 M thioanisole solutions. Thioanisole was purchased from Aldrich Chemical Co. The SEM image of the roughened Ag substrate was obtained using a Hitachi S-4800 microscope. The reflectance spectra were measured to determine the plasmon resonance ω_p.

The Raman spectra of thioanisole (concentration is 0.05 M) were recorded using the microprobe Raman system RH13325 (R-2000) spectrophotometer. A three-electrode cell was used to perform the oxidation–reduction cycles (ORCs). The sample was used as a working electrode, and a platinum wire was used as the counter electrode. An Ag/AgCl electrode was employed as the reference electrode. The applied voltages of the working electrode were controlled with a CHI619Belectrochemical instrument. The samples were excited with 532-nm and 785-nm lasers, and their effective powers were 0.15 and 1.27 mW, respectively. A 50× objective was used to achieve a 180°backward scattering configuration.

The theoretical calculations of the molecular Raman spectra and their vibrational modes were performed with the Gaussian 09 software using density functional theory[29], the B3LYP functional[30], and the 6-31G(d) basis set. The calculated Raman spectra were scaled according to Ref. 31.

1. Fleischmann, M., Hendra, P. J. & McQuillan, A. J. Raman spectra of pyridine adsorbed at a silver electrode. *Chem. Phys. Lett.* **26**, 163–166 (1974).
2. Jeanmaire, D. J. & Van Duyne, R. P. Surface Raman spectroelectrochemistry: Part I. Heterocyclic, aromatic, and aliphatic amines adsorbed on the anodized silver electrode. *J. Elektroanal. Chem.* **84**, 1–20 (1977).
3. Fan, X. *et al.* Light scattering and surface plasmons on small spherical particles. *Light: Sci. Appl.* **3**, e179 (2014).
4. Moskovits, M. Surface-enhanced spectroscopy. *Rev. Mod. Phys.* **57**, 783–826 (1985).
5. Sun, Q. *et al.* Direct imaging of the near field and dynamics of surface plasmon resonance on gold nanostructures using photoemission electron microscopy. *Light: Sci. Appl.* **2**, e118 (2013).
6. Otto, A., Mrozek, I., Grabhorn, H. & Akeman, W. Surface-enhanced Raman scattering. *J. Phys.: Condens. Matter.* **4**, 1143–1212 (1992).
7. Lombardi, J. R., Birke, R. L., Lu, T. & Xu, J. Charge-transfer theory of surface enhanced Raman spectroscopy: Herzberg–Teller contributions. *J. Chem. Phys.* **84**, 4174–4180 (1986).
8. Sun, M. T. *et al.* Remotely excited Raman optical activity using chiral plasmon propagation in Ag nanowires. *Light: Sci. Appl.* **2**, e112 (2013).
9. Sun, M. T. *et al.* Nanowire-supported plasmonic waveguide for remote excitation of surface-enhanced Raman scattering. *Light: Sci. Appl.* **3**, e199 (2014).
10. Xia, L. *et al.* Visualized method of Chemical Enhancement Mechanism on SERS and TERS. *J. Raman Spectrosc.* **45**, 533–540 (2014).
11. Fang, Y., Li, Y., Xu, H. & Sun, M. T. Ascertaining p,p'-dimercaptoazobenzene Produced from p-Aminothiophenol by Selective Catalytic Coupling Reaction on Silver Nanoparticles. *Langmuir.* **276**, 7737–7746 (2010).
12. Huang, Y. F. *et al.* When the signal is not from the original molecule to be detected: chemical transformation of para-aminothiophenol on Ag during the SERS measurement. *J. Am. Chem. Soc.* **132**, 9244–9246 (2010).
13. Christopher, P., Xin, H. & Linic, S. Visible-light-enhanced catalytic oxidation reactions on plasmonic silver nanostructures. *Nature.Chem.* **3**, 467–472 (2011).
14. Sun, M. T., Zhang, Z. L., Zheng, H. R. & Xu, H. X. In-situ plasmon-driven chemical reactions revealed by high vacuum tip-enhanced Raman spectroscopy. *Sci. Rep.* **2**, 647–651 (2012).
15. Lantman, E. M. van S., Deckert-Gaudig, T., Mank, A. J. G., Deckert, V. & Weckhuysen, B. M. Catalytic processes monitored at the nanoscale with tip-enhanced Raman spectroscopy. *Nature Nanotech.* **7**, 583–586 (2012).
16. Linic, S., Christopher, P., Xin, H. & Marimuthu, A. Catalytic and photocatalytic transformations on metal nanoparticles with targeted geometric and plasmonic properties. *Acc. Chem. Res.* **46**, 1890–1899 (2013).
17. Xu, P. *et al.* Mechanistic understanding of surface plasmon assisted catalysis on a single particle: cyclic redox of 4-aminothiophenol. *Sci. Rep.* **3**, 2997 (2013).
18. Sun, M. T., Zhang, Z. L., Kim, Z., Zheng, H. R. & Xu, H. X. Plasmonic Scissors for Molecular Design. *Chem. Eur. J.* **13**, 14958–14962 (2013).
19. Pincella, F., Isozaki, K. & Miki, K. A visible light-driven plasmonic photocatalyst. *Light: Sci. Appl.* **3**, e133 (2014).
20. Sun, M. T. *et al.* Plasmon-driven selective reductions revealed by tip-enhanced Raman spectroscopy. *Adv. Mater. Interfaces.* **1**, 1300125 (2014).
21. Kale, M. J., Avanesian, T. & Christopher, P. Direct Photocatalysis by Plasmonic Nanostructures. *ACS Catal.* **4**, 116–128 (2014).
22. Xie, W., Walkenfort, B. & Schlücker, S. Label-Free SERS Monitoring of Chemical Reactions Catalyzed by Small Gold Nanoparticles Using 3D Plasmonic Superstructures. *J. Am. Chem. Soc.* **135**, 1657–1660 (2013).
23. Urban, A. S. *et al.* Three-Dimensional Plasmonic Nanoclusters. *Nano Lett.* **13**, 4399–4403 (2013).
24. Zhang, X., Wang, P., Zhang, Z., Fang, Y. & Sun. M. Plasmon-driven sequential chemical reactions in an aqueous environment. *Sci. Rep.* **4**, 5407 (2014).
25. Liu, H. *et al.* Three-dimensional and time-ordered surface-enhanced Raman scattering hotspot matrix. *J. Am. Chem. Soc.* **136**, 5332–5341 (2014).
26. Govorov, A. O., Zhang, H. & Gunko, Y. K. Theory of Photoinjection of Hot Plasmonic Carriers from Metal Nanostructures into Semiconductors and Surface Molecules. *J. Phys. Chem. C* **117**, 16616–16631 (2013).
27. Arenas, J. F., Fernandez, D. J., Soto, J., Lopez, I. L. & Otero, J. C. Role of the Electrode Potential in the Charge-Transfer Mechanism of Surface-Enhanced Raman Scattering. *J. Phys. Chem. B* **107**, 13143–13149 (2003).
28. Brett, C. M. A. & Brett, A. M. O. *Electrochemistry: Principles, Methods and Applications,*(Oxford University Press, Oxford, England, 1993).
29. Parr, R. G. & Yang, W. *Density-functional theory of atoms and molecules* (Oxford Univ. Press, Oxford, 1989).
30. Lee, C., Yang, W. & Parr, R. G. Development of the Colle-Salvetti correlation-energy formula into a functional of the electron density. *Phys. Rev. B* **37**, 785–789 (1988).
31. Foresman, J. B. & Frisch, A. *Exploring Chemistry with Electronic Structure Methods* (Gaussian Inc. Pittsburgh, PA, USA, 2009).

Acknowledgments

This work was supported by the National Natural Science Foundation of China (Grant Nos. 91436102, 11374353, 21473115, 11474141, 11304135 and 11404055), National Key Basic Research Program of China (2014CB921001), the Program of Liaoning Key Laboratory of Semiconductor Light Emitting and Photocatalytic Materials, the Program of Shenyang Key Laboratory of Optoelectronic Materials and Technology (F12-254-1-00), Scientific Research Base Development Program of the Beijing Municipal Commission of Education, and Strategic Priority Research Program (B) of the Chinese Academy of Sciences (Grant No. XDB07030200).

Author contributions

M.S. and P.W. supervised the project, and M.S. designed the experiments. L.C. experimentally measured the SERS spectra. M.S., L.C., and P.W. analysed the data. M.S. wrote the paper, and X.C., Y.F., Z.Z., and Y.F. discussed and revised the manuscript.

Additional information

Competing financial interests: The authors declare no competing financial interests.

How to cite this article: Cui, L. *et al*. Plasmon-driven dimerization via S-S chemical bond in an aqueous environment. *Sci. Rep.* **4**, 7221; DOI:10.1038/srep07221 (2014).